Food Chemistry 218 (2017) 221–230

Contents lists available at ScienceDirect

Food Chemistry

journal homepage: www.elsevier.com/locate/foodchem

Gel characteristics and microstructure of fish myofibrillar protein/cassava starch composites

Mingcong Fan [a,b], Ting Hu [a,b], Siming Zhao [a,b], Shanbai Xiong [a,b], Jing Xie [c], Qilin Huang [a,b,*]

[a] College of Food Science and Technology, and MOE Key Laboratory of Environment Correlative Dietology, Huazhong Agricultural University, Wuhan 430070, China
[b] The Sub Center (Wuhan) of National Technology and R&D of Staple Freshwater Fish Processing, Wuhan 430070, China
[c] Hangzhou Starpro Starch Co. Ltd, Hangzhou 310016, China

ARTICLE INFO

Article history:
Received 19 April 2016
Received in revised form 6 September 2016
Accepted 11 September 2016
Available online 12 September 2016

Chemical compounds studied in this article:
Sodium chloride (PubChem CID: 5234)
Sodium dihydrogen phosphate (PubChem CID: 23673460)
Formaldehyde (PubChem CID: 712)
Ethanol (PubChem CID: 702)
Xylene (PubChem CID: 6850715)
Eosin (PubChem CID: 11048)
Iodine (PubChem CID: 807)

Keywords:
Fish myofibrillar protein
Cassava starch
Protein-starch composites
Starch fraction
Gel characteristics
Microstructure

ABSTRACT

The changes in fish myofibrillar protein/cassava starch composites in the starch fraction range from 0 to 1, with their total content maintained at 60 mg/mL, were investigated in terms of textural properties, rheological behaviours, morphology, spatial distribution and protein molecular structure. The results revealed that the starch fraction of 0.5 was a critical point for the conversion of the protein matrix to starch matrix and conversion of the gel from elastic to weak. Moreover, the protein-starch synergistic effect on the storage modulus was strongest at fractions of 0.5 and 0.6, due to the formation of a semi-interpenetrating network, with more amylose from the melted starch granules interpenetrated with the protein molecules, and the absorption of water by the starch granules to concentrate the protein matrix. Additionally, no covalent interaction between the protein and starch occurred with increasing starch fraction, thus having no significant influence on the protein secondary structure.

1. Introduction

Protein and starch, the essential biomacromolecules in food stuffs, not only supply necessary nutrition but are also responsible for the formation of characteristic textures due to their abilities to form gels (Joshi, Aldred, Panozzo, Kasapis, & Adhikari, 2014). It has been commonly accepted that protein and polysaccharide interact with each other when brought together (Alvarez, Fernández, Olivares, & Canet, 2012; Jekle, Mühlberger, & Becker, 2016). Moreover, these interactions influence the macro-properties and the micro-structures of their composites in terms of texture, stability, rheological properties, and chemical structure. Surimi has gained wide attention owing to several of its characteristics, including its high protein, low fat, ready-to-eat nature and unique texture (Muriel-Galet, López-Carballo, Gavara, & Hernández-Muño, 2015). Fish myofibrillar protein (MP) plays a major role in the gelation and texture of surimi. Starch is the second most important ingredient used in the manufacture of surimi products (Hunt, Getty, & Park, 2009). Hence, a thorough understanding of the interaction between MP and starch is crucial for elucidating structure and function relationships in surimi foods.

For an ideal mixture of protein and polysaccharide without intermolecular interactions, the property of the composite can be expressed as a linear summation of its components (Van Ness & Abbott, 1982). A study of pork ham batter/starch composites revealed that they exhibited higher rheological properties than did the linear combination of their components, indicating a synergistic effect between pork ham batter and gelatinized starch (Li & Yeh, 2002). Moreover, starches (potato starch, corn starch and rice

* Corresponding author at: College of Food Science and Technology, and MOE Key Laboratory of Environment Correlative Dietology, Huazhong Agricultural University, Wuhan 430070, China.
E-mail addresses: hql@mail.hzau.edu.cn, whuhql@gmail.com (Q. Huang).

http://dx.doi.org/10.1016/j.foodchem.2016.09.068
0308-8146/

starch) and salt-soluble protein composites exhibited a reinforcement effect, which might depend on starch granule size and composite structure (Li & Yeh, 2003). Additionally, corn starch and soy protein concentrate displayed an antagonistic effect, manifested in composites that showed lower rheological properties than did the linear combination of their components (Li, Yeh, & Fan, 2007). Based on the aforementioned studies, the value of α is introduced in the present work for quantification of the synergistic or antagonistic effect in a mixture of fish MP and cassava starch (CS).

Currently, most research efforts are focused on optimizing the starch type, concentration, and modification methods to develop the most effective starch for improving the gel strength of surimi (Sun, Huang, Hu, Xiong, & Zhao, 2014; Yang, Wang, Wang, & Ye, 2014). High gel strength is a high priority for surimi products, but with this strength comes an inability to satisfy the demands of consumers with a preference for soft texture, especially the elderly and children. Accordingly, the demand from these consumers suggests a necessity for surimi products with a weak gel strength. Surimi gel strength can be increased by adding a small amount of starch, but little information is available about the case with a large amount of starch added or even with starch as the dominant component. In a preliminary experiment, when CS was substituted for MP as the major component, MP/CS composites formed a weaker gel than single MP, which provides a new approach for developing soft surimi gel to satisfy special consumer needs.

The objectives of the present study were to elucidate the effects of the CS fraction (χ_{cs}) on gel properties and the interaction of MP/CS composites and to explore the change in the secondary structure of MP from grass carp under the macromolecular environment of CS. Specifically, MP from grass carp was mixed with CS at χ_{cs} values varying from 0 to 1 to obtain composites from MP to CS matrix and then heated in two steps to prepare gel samples. The texture of the MP/CS gels was measured by a texture analyser; the spatial partitioning of MP and CS in the composite gels was observed by an optical microscope with eosin/iodine double-staining; the viscoelasticity and compliance of MP/CS mixtures were monitored using a dynamic rheometer with temperature ramp and creep-recovery patterns; the effect of the CS fraction on the MP secondary structure was determined by Fourier transform infrared-attenuated total reflection (FTIR-ATR) spectroscopy. This work not only reveals the synergistic reinforcement effect between fish MP and CS but also provides a basis for the development of specific surimi products to satisfy special consumer needs.

2. Materials and methods

2.1. Materials

Grass carp (*Ctenopharyngodon idellus*) was purchased from Huazhong Agricultural University in Wuhan, Hubei, China. The cassava starch (CS) was provided by Hangzhou Starpro Starch Co. Ltd (Hangzhou, Zhejiang, China). Its contents of moisture, crude protein, lipid and ash of the CS sample were determined to be 10.0, 0.5, 0.3 and 0.5%, respectively, by AOAC (Association of Official Analytical Chemists) methods (1990). All chemicals used were of analytical grade.

2.2. Extraction of myofibrillar protein (MP) from grass carp

Myofibrillar protein (MP) was extracted from grass carp as described in our previous work (Sun et al., 2014). Briefly, fish mince was rinsed with a low-salt phosphate buffer (0.05 M NaCl, 3.38 mM $NaH_2PO_4{\cdot}2H_2O$, 15.5 mM $Na_2HPO_4{\cdot}12H_2O$, pH 7.5) to remove the water-soluble protein and other substances. Subsequently, the obtained pellets were extracted at 4 °C with a high-salt phosphate buffer (0.45 M NaCl, pH 7.5). After centrifugation, the supernatant was poured into deionized water at 4 °C to precipitate MP. Finally, the precipitate (MP) was collected by centrifugation. The MP concentration was measured using the Lowry method, with serum albumin used as a standard. The activities of endogenous transglutaminase (TGase) and cathepsins B and L were determined as described as Yongsawatdigul, Worratao, and Park (2002) and Jiang, Lee, Tsao, and Li (1997), respectively.

2.3. Preparation of myofibrillar protein/cassava starch (MP/CS) composites

The MP was dissolved using a phosphate buffer (0.6 M NaCl, pH 7.5), and CS was dispersed in the same buffer; then, the two were mixed at various CS fractions (χ_{cs} 0, 0.1, 0.2, 0.3, 0.4, 0.5, 0.6, 0.7, 0.8, 0.9 and 1), with the total content of MP plus CS maintained at 60 mg/mL. The MP/CS liquid mixtures (except for the pure CS sample with χ_{cs} 1) were stirred for 30 min and then centrifuged at 4 °C, 800 r/min for 5 min to remove the bubbles for rheological tests.

To prepare MP/CS gels, the as-prepared MP/CS liquid mixtures were poured into a casing with a diameter of 15 mm and then heated using a two-step procedure, i.e., 40 °C for 60 min followed by 90 °C for 30 min (Arfat & Benjakul, 2012; Sun et al., 2014). Finally, a series of cylindrical MP/CS composite gels were obtained and cooled to room temperature for texture, light microscopy and FTIR-ATR analysis. The single MP and CS samples corresponding to the MP/CS composites were also prepared and analysed.

2.4. Transparency measurement

The gel transparency was measured between 200 and 800 nm using a UV/Visible spectrophotometer (UV-1800, Shimadzu, Japan) as reported by Nuanmano, Prodpran, and Benjakul (2015). The transparency was calculated using the following equation:

$$\text{Transparency} = \frac{A_{600}}{X} \text{ or } -\frac{\text{Log } T_{600}}{X} \quad (1)$$

where A_{600} and T_{600} are absorbance and transmittance at 600 nm, respectively. X is gel thickness.

2.5. Textural profile analysis (TPA)

Textural profile analysis (TPA) of the MP/CS gels was performed on a texture analyser (TA-XT. Plus, Stable Micro Systems, UK) equipped with probe P/36R. The gels were cut into cylinders with a diameter of 15 mm and a height of 20 mm and then compressed at a compression degree of 50% with both the pre-test and test speed set at 1 mm/s and the post-test speed set at 5 mm/s. The trigger type was set to auto with a 5.0 g trigger force. All samples measurements were performed in decuplicate and repeated twice.

2.6. Rheological tests

Rheological tests, including temperature ramp and creep-recovery, were conducted on an AR2000ex stress-controlled rheometer (TA Instruments Ltd., Crawley, UK) equipped with a Peltier device for temperature control and a parallel-plate geometry (diameter 40 mm, gap 1 mm). The exposed samples were covered with a cap that was coated with liquid paraffin to avoid sample dehydration. All measurements were performed in the linear viscoelastic region, which was determined by stress sweeps within a 0.1–10 Pa range.

2.6.1. Temperature ramp test

The temperature ramp tests on the MP/CS composites and the corresponding single MP and CS samples were carried out as follows: heating from 20 to 90 °C at 2 °C/min and then cooling to 20 °C at 5 °C/min. All tests were conducted at 1 Hz and 1 Pa in the linear viscoelastic region. The storage modulus (G′) was determined using the rheometer data-analysis software (Ding et al., 2012).

2.6.2. Creep-recovery test

Creep-recovery tests on the pure MP samples were carried out at 4, 20, 40, 50, 60 and 80 °C, and the MP/CS composites prepared with χ_{cs} values of 0, 0.2, 0.5 and 0.8 were tested at 80 °C. In the creep phase, samples were subjected to 0.2 Pa within the linear viscoelastic region, and the strain in response to the constant stress was measured over 180 s. In the recovery phase, the applied stress was suddenly removed, and the sample recovery was recorded for 420 s. The effects of temperature and χ_{cs} on the creep-recovery characteristics of the MP/CS composites were represented using Burger's model (Juszczak et al., 2012).

2.7. Light microscopy with eosin/iodine double-staining

The morphology and distribution of MP and CS in the composite gels were detected using light microscopy with eosin/iodine double-staining as described by Chiang, Li, and Chen (2009). The MP/CS composite gels, with pure MP and CS gels used for comparison, were fixed in a 10% formalin solution. After that, the samples were dehydrated by immersion separately in a series of graded ethanol solutions and xylene and then embedded in paraffin. A serial section 4 μm thick was obtained using a microtome (RM-2016, Leica, German), then mounted on a slide, and finally deparaffined with xylene. The deparaffined section was stained with eosin and MP was indicated in red. The subsequent staining with the iodine solution resulted in pink for the protein and dark blue or purple for the CS. The distributions of MP and CS in the samples were observed using a light microscope (Eclipse CI, Nikon, Tokyo, Japan) equipped with a 35 mm photomicrography camera (Microflex HFX-IIA, Nikon, Tokyo, Japan).

2.8. Fourier transform infrared-attenuated total reflection spectroscopy (FTIR-ATR)

FTIR spectra of the MP/CS composites were recorded on an FTIR spectrophotometer (Nexus 470, Nicolet, UK) equipped with a universal ATR attachment and collected over a 400–4000 cm^{-1} range using an average of 64 scans and 4 cm^{-1} resolution. Curve fitting procedures were used to deconvolute the amide bands observed in the 1600–1700 cm^{-1} range, as reported by Mejia, Mauer, and Hamaker (2007). The spectra were normalized by applying a multipoint linear base-line correction using the PeakFit software (Version 4.12) and then were curve fit with a Gaussian-Lorentzian mixed function. The iterative data fitting was performed until an R^2 value of 0.99 was achieved. The relative peak areas of the absorbance bands were expressed as "the percentage of the area of the fitted region". Fourier deconvoluted spectra can verify the changes in the MP secondary structure caused by addition of CS and its fractions.

2.9. Statistical analysis

All tests, unless otherwise stated, were performed in triplicate and repeated three times, and the data were presented as the means ± SD (standard deviation). The creep data were modelled according to the Burger's model, using the non-linear regression feature in Microsoft Excel 2003.

3. Results and discussion

3.1. Transparency and textural properties of MP/CS composite gels

The photographs of the MP/CS composite gels are shown in Supplement Fig. 1, and the transparency is listed in Supplement Table 1. A higher value of A_{600}/mm represents lower transparency (Nuanmano et al., 2015). When χ_{cs} increased from 0 to 1, the value of A_{600}/mm decreased from 14.30 to 1.25, indicating that the transparency of MP/CS gels increases as χ_{cs} is elevated. The transparency and profile of the composite gels were obviously influenced by χ_{cs}. The high-MP composite gels ($\chi_{cs} \leqslant 0.5$) formed elastic gels with well-formed dimensions, whereas the high-CS composite gels ($\chi_{cs} \geqslant 0.6$) exhibited a weak character with an unstable shape. As for the pure CS sample (χ_{cs} 1), the concentration of 60 mg/mL did not reach the level required to form a gel with a stable shape during heating and subsequent cooling, thus showing typical characteristics of a viscous fluid. When χ_{cs} increased from 0 to 1, the morphology of the MP/CS composite gels transformed from MP gel → MP/CS elastic gel → MP/CS weak gel → CS viscous fluid, suggesting that the CS fraction and total content of MP plus CS were crucial for the expression of gelation characteristics and that χ_{cs} 0.5 might be a critical point for the gel morphology transitioning from elastic to weak.

The high-MP composite gels ($\chi_{cs} \leqslant 0.5$) were selected for textural profile analysis (TPA) because of their stable shape, and the TPA parameters are summarized in Supplement Table 2. The CS fraction had a significant influence on hardness, adhesiveness, gumminess and chewiness of the MP/CS composite gels ($P < 0.05$), which decreased from 311.24 to 137.10 g, −35.14 to −13.29 g·s, 189.86 to 87.74, and 174.04 to 79.03, respectively, as χ_{cs} increased from 0 to 0.5. Such changes were probably attributed to two reasons. First, the decrease in the MP content from 60 to 30 mg/mL led to the weak gel formation capability of the MP matrix. Second, when the CS content increased from 30 to 60 mg/mL, its ability to form a gel network by itself was much weaker than that of MP at the same concentration, implying that the increase in CS could not completely compensate for the decrease of MP gel formation capability, even though the CS granules as filler might reinforce the MP gel matrix to some extent (Yang & Park, 1998). Therefore, the effect of MP on the whole network structure of the MP/CS gels was more remarkable than that of CS due to the gel matrix produced by MP. Springiness is a textural attribute related to the rapidity and degree of recovery from a deforming force (Di Monaco, Cavella, & Masi, 2008). The springiness was not significantly different among the gel samples ($p > 0.05$), suggesting that it was not sensitive to the protein/starch ratio. A similar phenomenon also occurred in a series of lentil protein/starch gels with different starch fractions (Joshi et al., 2014). This can be explained by the fact that the CS gelatinization contributed to the elasticity of the MP/CS composite gels, thereby compensating for the springiness reduction caused by the decreased MP content. Cohesion is a direct function of the work needed to overcome the internal bonding of the gel network (Friedman, Whitney, & Szczesniak, 1963). The values of cohesion increased slightly as χ_{cs} increased from 0 to 0.5, indicating that the internal bonds of the composite gel became stronger. The temperature ramp tests also supported the assertion that the synergistic effect between MP and CS was enhanced with increasing χ_{cs}.

3.2. Rheological properties of MP/CS composites

3.2.1. Temperature ramp test

The rheological properties of the MP/CS composites were monitored by temperature ramp tests during a heating and cooling

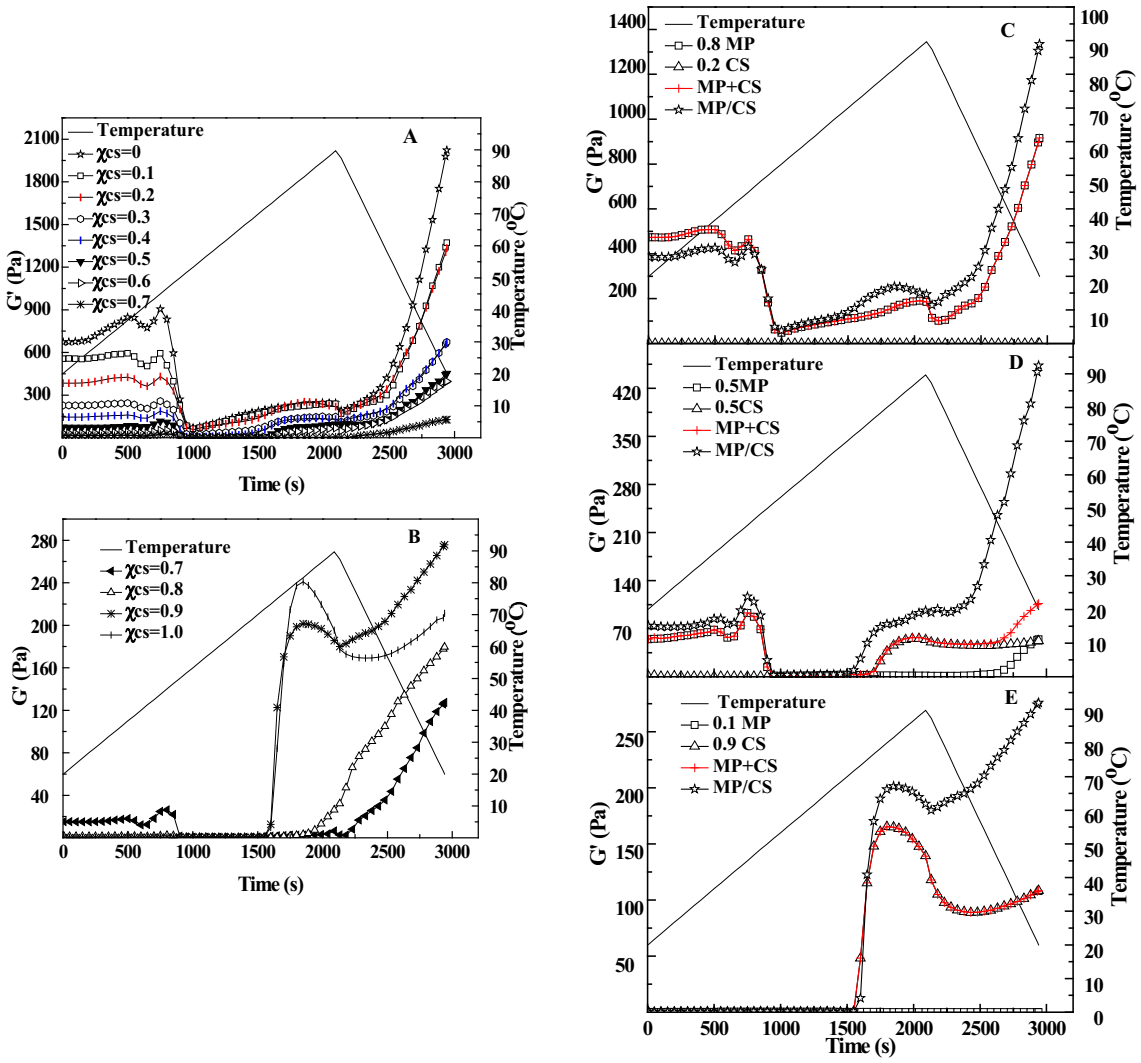

Fig. 1. Plots of storage modulus G′ vs. time for MP, CS, MP + CS[a] and MP/CS[b] with different χ_{cs}^{c} in temperature ramp test. [a]G′(MP + CS) was calculated as a linear combination of G′(MP) and G′(CS). [b]G′ (MP/CS) was the experimental data of MP/CS composites. [c]A–B: χ_{cs} = 0–1; C: χ_{cs} = 0.2; D: χ_{cs} = 0.5; E: χ_{cs} = 0.9.

cycle (20 °C → 90 °C → 20 °C). Fig. 1(A–B) contain plots of G′ vs time for the MP/CS composites. For the pure MP sample (χ_{cs} 0), G′ increased slowly with temperature from 20 to 45 °C, and peaked at ~45 °C; with further heating, G′ dropped sharply to a minimum at ~53 °C; finally, G′ presented a second increase as the temperature rose from 53 to 90 °C (Sun et al., 2014). G′ within the 20–90 °C temperature range showed a consistent trend with the typical thermal behaviours of surimi: suwari-modori-kamaboko (Foegeding, Allen, & Dayton, 1986). For the pure CS sample (χ_{cs} 1), a peak value of G′ occurred in the 70–90 °C temperature range due to starch gelatinization. Based on thermal rheological behaviours, the MP/CS composites could be classified into MP-dominated composites (χ_{cs} 0.1–0.7) and CS-dominated composites (χ_{cs} 0.8 and 0.9). The former exhibited similar rheological behaviours to the pure MP (suwari-modori-kamaboko) and G′ (at 90 °C) decreased with decreasing MP fraction, while the gelatinization peak of CS was not obvious. The latter showed a starch-like pasting curve, and the G'_{peak} increased with increasing CS fraction, although no thermal behaviour typical of MP was observed. Therefore, the rheological behaviours of MP/CS composites were remarkably affected by the domination of either MP or CS (Joshi et al., 2014). Additionally, as the temperature decreased from 90 to 20 °C, all samples exhibited a sharp rise in G′, indicating that the gel network could be strengthened through cooling. During cooling, both the protein and the starch molecules would reassociate and form gels individually through non-covalent interactions (hydrogen bonds, nonspecific associations etc.) (Ashwar, Gani, Shah, Wani, & Masoodi, 2015; Jia, Huang, & Xiong, 2016). Especially for starch gels, non-covalent interactions were generally believed to involve the formation of an intermolecular double helix stabilized by hydrogen bonding (Ashwar et al., 2015).

The properties of an ideal mixture (or solution) without intermolecular forces between components can be expressed as a linear summation of its components (Van Ness & Abbott, 1982). In this study, the plots of G′ vs time for MP + CS were obtained using a linear summation of the corresponding MP and CS plots using Eq. (2). The value of α was introduced as represented by Eq. (3) to evaluate whether a synergistic enhancement or an antagonistic effect occurred in the MP/CS mixture. If α > 1, MP and CS exhibit a synergistic enhancement; if α = 1, MP and CS have no interaction; if α < 1, MP and CS exhibit an antagonistic effect.

$$G'(MP + CS) = G'(MP) + G'(CS) \quad (2)$$

$$\alpha = G'_{end}(MP/CS)/G'_{end}(MP + CS) \quad (3)$$

where G'_{end} (MP), G'_{end} (CS) and G'_{end} (MP/CS) are obtained at the final cooling temperature of 20 °C for pure MP, pure CS and the MP/CS composites. Fig. 1(C–E) shows plots of G′ vs time for MP, CS, MP + CS and MP/CS. At a χ_{cs} of 0.2, G′ of MP/CS (the experimental data) started to exceed that of MP + CS (the linear summation data) from 68.3 °C and this trend continued up to subsequent cooling, suggesting a synergistic enhancement between MP and CS. Moreover, a maximum G′ value appeared between 68.3 and 87.4 °C for MP/CS, due to CS gelatinization. The starch gelatinization in surimi was necessary for the firmness and gel strength of the products (Li & Yeh, 2002). The reinforcing effects of starch might be explained by the fact that starch granules embedded in the protein matrix would absorb water and swell to compress the protein, resulting in moisture loss and a firmer matrix (Kim & Lee, 1987). At a χ_{cs} of 0.5, the MP/CS showed both MP rheological and CS gelatinization characteristics and had a higher G′ than a simple MP + CS linear summation throughout heating and cooling. Especially after cooling, G′ of MP/CS increased much more quickly than that of MP + CS, suggesting a higher synergistic effect. At a χ_{cs} value of 0.9, the MP thermal rheological behaviour was not detected, but CS gelatinization was obvious. Similar synergistic reinforcement was also found at χ_{cs} 0.9. Such a synergistic reinforcement could be quantified by the α value (Table 1(A)). For all the MP/CS composites, the α values were greater than 1, indicating a synergistic reinforcement in all the MP/CS composites under heating and cooling. It is worth noting that the reinforcement effect was the strongest at χ_{cs} 0.5 and 0.6 with α values of 4.24 and 5.89, attributed to the stronger interaction between MP and CS at the phase transformation from the MP matrix to the CS continuous phase, which was further confirmed by the following morphology observation with eosin/iodine double-staining.

3.2.2. Creep-recovery test

Creep behaviour can be estimated by the Burger's model in terms of compliance. The relation between deformation amount per unit stress (compliance, J) and time is expressed by the following equation (Juszczak et al., 2012):

$$J(t) = J_0 + J_1\left(1 - \exp\left(-\frac{t}{\lambda}\right)\right) + \frac{t}{\eta_0} \quad (4)$$

where J(t) represents the overall compliance at any time t; J_0 is the instantaneous elastic compliance; J_1 is the retarded elastic compliance; λ is the retardation time and η_0 is the zero shear viscosity.

Fig. 2(A–B) show the creep-recovery curves of the MP samples at different temperatures (4, 20, 40, 50, 60 and 80 °C). Compliance at the end of the creep phase (J_{max}) reflects the maximum resistance to deformation as an indicator of the bond strength between the structure units (Onyango, Mutungi, Unbehend, & Lindhauerc, 2010). A lower J_{max} value represents greater resistance to deformation and stronger material structure. J_{max} decreased as the temperature increased from 4 to 40 °C, verifying that endogenous TGase strengthened the protein–protein interaction through an ε-(γ-glutamyl) lysine cross-link to induce pre-gelation as found in our previous work (Ding et al., 2012; Jia et al., 2016). In this work, TGase activity of fresh grass carp meat was 482.7 U/g, and that of the MP sample was 72.4 U/g (~15% of the original TGase activity). Additionally, the TGase activity increased with temperature from 4 to 45 °C, and peaked at ~45 °C. Thus, the cross-linking catalysed by TGase would occur in the MP sample to induce MP gelation within the 4–45 °C temperature range. However, at 50 °C, J_{max} jumped to the highest value (0.15 Pa^{-1}), due to modori (i.e., the break-down of the loose gel network caused by heat-activated proteases, especially cathepsins B and L that exhibited a high activity and degraded myosin at 45–53.3 °C) (Jiang, Lee, Tsao, & Li, 1997). Through the MP preparation, 12.18 and 30.76% of cathepsins B and L still remained, respectively, in contrast to their respective activity of 0.68 and 0.82 U/g in fresh grass carp. Subsequently, J_{max} reduced again with the temperature from 50 to 80 °C, indicating a reinforcement of MP gel structure with increasing temperature in kamaboko, owing to the disulfide covalent bonding and hydrophobic interactions (Jia et al., 2016).

Fig. 2(C) shows the creep-recovery curves of the MP/CS composites at 80 °C. Table 1(B) summarizes the values of J_0, J_1, λ and η_0 obtained by fitting the creep data to the Burger's model. The Burger's model gave the best fit to the creep data ($R^2 > 0.90$), suggesting that the model was sufficient to describe the viscoelastic property and reflect the internal structure of the MP/CS composites. The creep-recovery behaviour is associated with the reorientation of bonds in viscoelastic materials (Onyango et al., 2010). The instantaneous elastic compliance (J_0) is closely related to the elastic stretching energy of primary bonds, such as ionic and covalent bonds, that are damaged irreversibly, whereas the retarded elastic compliance (J_1) is characterized by the breakage and transformation of secondary bonds, such as van der Waals interactions, that are destroyed reversibly when the stress is applied and then removed (Rao, Kash, Cooley, & Barnard, 1987). Obviously, J_0 varied slightly as χ_{cs} increased from 0 to 0.2, but it increased rapidly up to the maximum (15.22×10^{-3} Pa^{-1}) at χ_{cs} 0.5 and then dropped sharply to the minimum (5.72×10^{-3} Pa^{-1}) at χ_{cs} 0.8. J_1 followed the same tendency as J_0. When the MP fraction (χ_{mp}) decreased from 1 to 0.5, the number of ε-(γ-glutamyl) lysine and disulfide covalent bonds decreased and secondary bonds such as hydrophobic interactions weakened, leading to higher J_0 and J_1, indicating that the MP/CS composites had less resistance to deformation. When χ_{cs} increased to 0.8, CS formed a continuous phase and its gelatinization prevailed, resulting in the sharp drops of both J_0 and J_1. Notably, the retardation time (λ) characterizes the response of a viscoelastic material to the instantaneous application of a constant stress (Juszczak et al., 2012). A longer retardation time represents a slower elastic response (Ronda, Pérez-Quirce, Angioloni, & Collar, 2013). The retardation time λ increased as χ_{cs} increased from 0 to 0.8 (especially χ_{cs} from 0.2 to 0.5), indicating a slower

Table 1A
Dynamic rheological properties of MP, CS, MP + CS and MP/CS composites with different CS fractions (χ_{cs} 0.1–0.9) in temperature ramp test.

CS fraction (χ_{cs})	G'_{end} (MP) (Pa)	G'_{end} (CS) (Pa)	G'_{end} (MP + CS)[a] (Pa)	G'_{end} (MP/CS)[b] (Pa)	α
0.1	1349.0	0.038	1349.0	1372.0	1.010
0.2	916.1	0.116	916.2	1334.0	1.456
0.3	575.9	22.3	598.2	672.9	1.125
0.4	388.4	46.8	435.2	670.0	1.540
0.5	54.6	52.1	106.7	452.0	4.235
0.6	12.7	54.6	67.3	396.2	5.890
0.7	3.102	70.1	73.2	127.4	1.740
0.8	2.504	88.5	91.0	179.6	1.973
0.9	0.099	108.3	108.4	275.8	2.544

[a] G'_{end} (MP + CS) was calculated as a linear combination of G'_{end} (MP) and G'_{end} (CS).
[b] G'_{end} (MP/CS) was the experimental data of MP/CS composites.

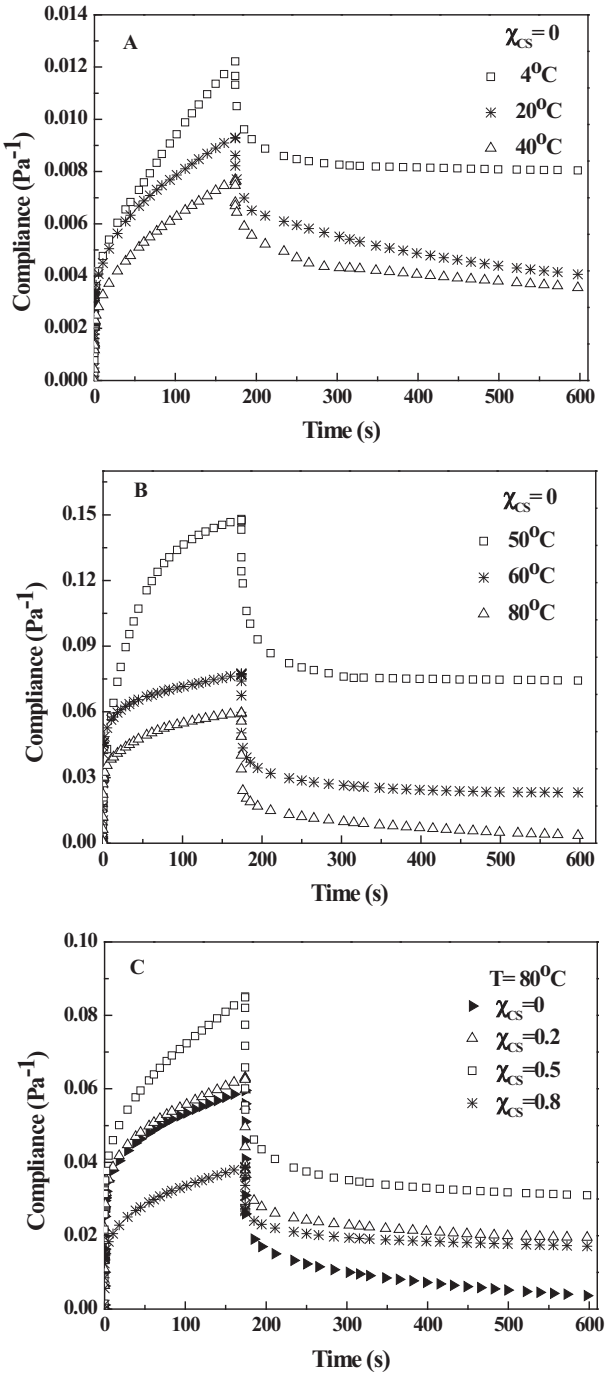

Fig. 2. Creep-recovery curves of MP and MP/CS composites affected by temperature (A–B) and χ_{cs} (C), respectively.

elastic response and increased difficulty in reorienting structural elements, which resulted in a lower recovery rate after deformation. The zero shear viscosity (η_0) reflects flowability of the material at the end of the creep phase, representing the linear region of Newtonian compliance in which the units flow past one another, as a result of the rapture of bonds (Rao et al., 1987). The lowest and highest η_0 values for the MP/CS composites (24.55×10^3 and 65.55×10^3 Pa·s) were observed at χ_{cs} 0.5 and 0.8, respectively, suggesting the lower flowability of the MP/CS composites at the higher χ_{cs}, which might be due to the water absorption and gelatinization of a large amount of CS resulting in a high viscosity.

The two fundamental components of the compliance (reversible and irreversible) can be identified as follows. The reversible compliance contains the instantaneous (J_0) and retarded (J_1) elastic compliance. The irreversible compliance (J_v) is due to the viscous flow of the material ($J_v = t/\eta_0$ or $J_{max} - (J_0 + J_1)$) over larger time scales. The recovery (R%) of the entire system is expressed as the percentage of the reversible compliance to the maximum compliance as follows (Onyango et al., 2010):

$$\text{Recovery } (R\%) = \frac{(J_0 + J_1)}{J_{max}} \times 100\% \quad (5)$$

Despite significant changes in the Burger's model parameters (J_{max}, J_0 and J_1 etc.) at various CS fractions, the recovery only slightly changed within 76.5–82.3%. J_1 represented the largest contribution (60.0–67.5%) to the total compliance, followed by J_0 (14.8–20.2%) and J_v (17.7–23.5%). This result suggested that the MP/CS composite system exhibited a more solid-like behaviour with high elasticity and resistance to deformation because MP and CS could individually form a gel network after heating. During the transition from the MP matrix to the CS continuous phase, the CS gel could partially replace the MP gel and maintain the elasticity and the strength of the MP/CS gel network.

3.3. The spatial distributions of MP and CS in composite gels

The distributions of MP and CS in the MP/CS composite gels were observed by light microscopy with eosin/iodine double-staining (Fig. 3). As shown by single-staining, the pure MP (red colour) and CS (dark blue) samples both formed a compact and homogeneous phase (Fig. 3A and B). As χ_{cs} increased from 0 to 0.5, MP still presented a continuous phase (Fig. 3C, E and G) and formed the backbone of the network, due to the binding effect of MP and the low denaturation temperature (Chiang et al., 2009). With the addition of CS granules, many approximately circular voids were observed in the MP matrix, and the number of the voids remarkably increased with increasing χ_{cs} (Fig. 3C, E, G and I). Perhaps because of the free availability of water, the starch granules swelled and became disrupted during gelatinization, leading to the generation of the main voids. The size of the voids was usually larger than the size of the intact starch granules, attributed to the swelling of the starch (Kim & Lee, 1987), as well as the decrease in the total protein concentration.

MP and CS were double-stained to further elucidate their structural morphology in the composites. As shown in

Table 1B
The parameters of Burger's model for MP/CS composites with different χ_{cs} in creep-recovery test.

CS fraction (χ_{cs})	$J_0 \times 10^{-3}$(Pa^{-1})	$J_1 \times 10^{-3}$(Pa^{-1})	λ (s)	$\eta_0 \times 10^3$ (Pa·S)	$J_{max} \times 10^{-3}$(Pa^{-1})	R (%)
0	12.01 ± 0.71b	36.25 ± 0.71b	2.06 ± 0.07b	32.78 ± 0.00b	59.59 ± 0.07c	81.00 ± 2.37a
0.2	10.39 ± 0.87b	37.88 ± 1.66b	3.92 ± 0.17b	32.78 ± 0.00b	63.13 ± 0.14b	76.46 ± 1.25a
0.5	15.22 ± 0.44a	53.02 ± 4.24a	14.74 ± 0.00a	24.55 ± 0.00c	85.10 ± 1.41a	80.20 ± 4.47a
0.8	5.72 ± 0.72c	26.16 ± 1.47c	15.10 ± 4.54a	65.55 ± 0.00a	38.74 ± 1.00d	82.27 ± 1.93a

Mean values with different lowercase letters (a–c) of each row differ significantly ($P < 0.05$).

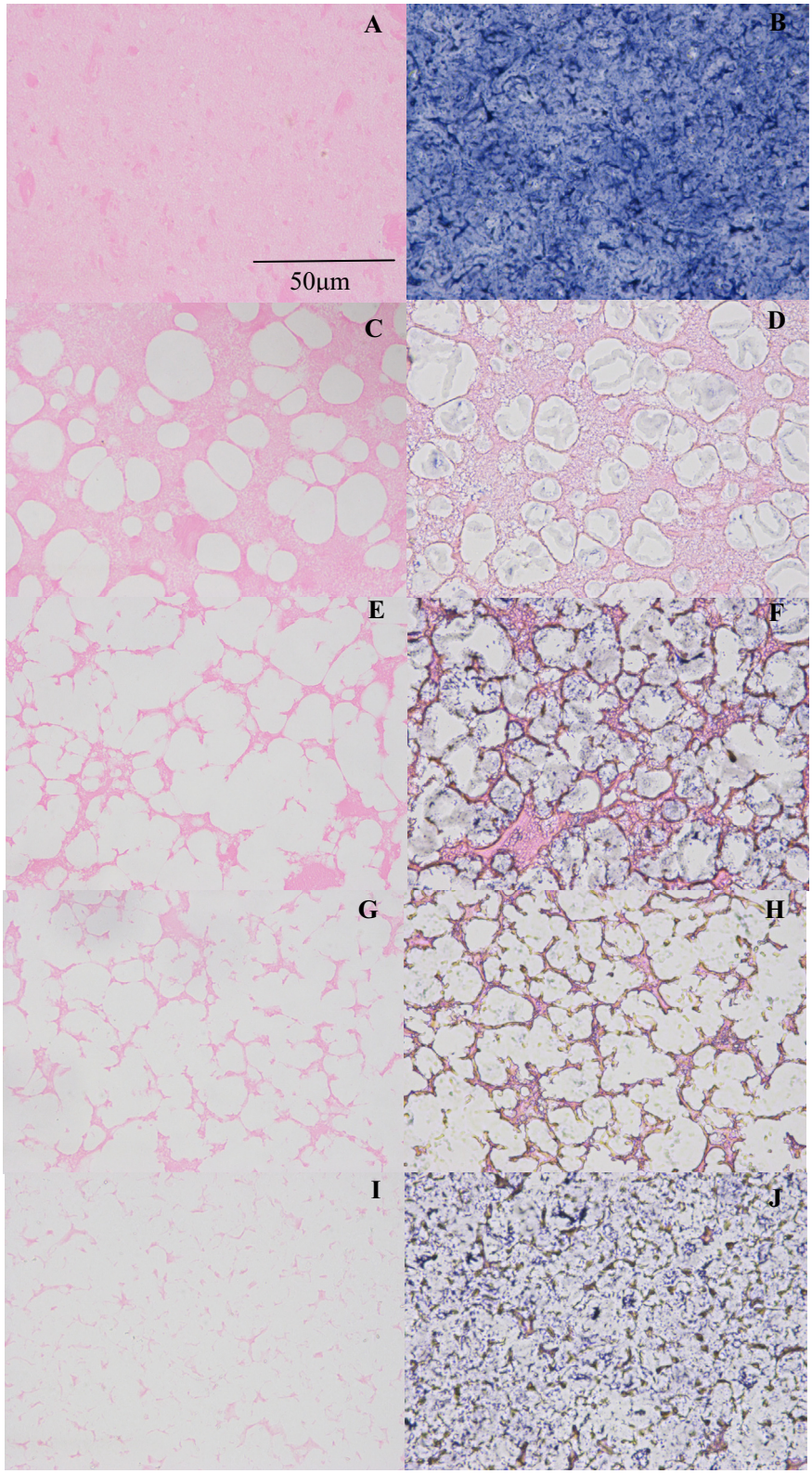

Fig. 3. Light micrographs for MP, CS, and MP/CS composite gels with different χ_{cs} after eosin-staining (A, C, E, G and I), iodine-staining (B) and eosin/iodine double-staining (D, F, H and J) A: χ_{cs} = 0; B: χ_{cs} = 1; C, D: χ_{cs} = 0.2; E, F: χ_{cs} = 0.5; G, H: χ_{cs} = 0.6; I, J: χ_{cs} = 0.8. Protein in red as stained with eosin; starch in dark blue as stained with iodine. (For interpretation of the references to colour in this figure legend, the reader is referred to the web version of this article.)

Fig. 3D, F, H and J, the distribution and morphology of starch presented three forms: filled in the voids, coated on the peripheral surface of the protein network or trapped in the protein network. At χ_{cs} 0.2 (Fig. 3D), most of the gelatinized starch either filled the voids or coated the peripheral surface of protein network, while a small part of starch was trapped in the protein network, due to the leaching of amylose from the melted starch granules into the protein matrix. At χ_{cs} 0.5 (Fig. 3F), more amylose was

released from the starch granules into the protein matrix and interpenetrated with protein molecules. With a further increase in χ_{cs} (χ_{cs} 0.6 in Fig. 3H), some breakage occurred in the protein network, and the continuous phase was difficult to define, with more and more starch embedded in the protein network or attached to the interface between the protein and the void, and without gelatinized starch observed in the network voids. At χ_{cs} 0.8 (Fig. 3J), the breakage was too severe in the MP network to form an integrated network. Conversely, CS formed a continuous phase instead of MP.

Generally, protein-polysaccharide mixtures are thermodynamically incompatible at neutral pH, which causes a phase separation and the formation of a two-phase system. In the two-phase system, the filler existed as dispersed liquid particles or a secondary gel network, and it was presumably unassociated with the continuous phase (Wu et al., 2015; Ziegler & Foegeding, 1990). A binary mixture of MP and CS was defined as a two-phase gel (Park, 2005): both components underwent gel transition independently and were capable of forming a continuous gel network. Whether MP or CS contributed to a continuous phase in the two-phase system depended upon the MP/CS ratio, and the phase inversion occurred at χ_{cs} 0.5, which was also found in cereals protein and starch (Chanvrier, Colonna, Della Valle, & Lourdin, 2005). Furthermore, the interpenetration between amylose and the MP molecules was more clearly observed at χ_{cs} 0.5 and 0.6. The formation of such an interpenetrating network in a local region (or a semi-interpenetrating network) was probably responsible for the synergistic effect of MP and CS in the reinforcement of G′.

3.4. Molecular structures of MP/CS composites

Fig. 4(A) displays the FTIR spectra of MP, CS and the MP/CS composite gels. The pure MP sample (χ_{cs} 0) showed strong and broad bands in the 3200–3600 cm^{-1} region, ascribed to intermolecular H-bonded N—H and O—H stretching vibration. The weak peak at 2931 cm^{-1} was attributed to the C—H stretching vibration. Typical protein bands at 1655, 1540, 1402 and 1240 cm^{-1} are associated with amide I (80% C=O stretch, 10% C—N stretch), amide II (60% N—H bend, 30% C—N stretch and 10% C—C stretch), and amide III (complex bands resulting from several coordinate displacements) (Kaddour, Mondet, & Cuq, 2008). For the pure CS sample (χ_{cs} 1), the peaks at 3438 cm^{-1} and 2931 cm^{-1} were assigned to O—H and C—H stretching. The absorption peak at 1639 cm^{-1} might be due to the stretching of the glucose ring (Rashid, Al Omari, Leharne, Chowdhry, & Badwan, 2012). The bands in the 800–1200 cm^{-1} region (1158, 1080, 1020, 931, 855 cm^{-1}) can be used as a "fingerprint" for starch, dominated by ring vibrations overlapped by C—OH, C—C and C—H side group vibrations and the C—O—C glycosidic bond vibration (Kacurakova, Capek, Sasinkova, Wellnerb, & Ebringerová, 2000). Obviously, only the peaks of MP and CS appeared in the spectra of the MP/CS composite gels (χ_{cs} 0.2–0.8), indicating no chemical interaction (covalent bond) between MP and CS during heating.

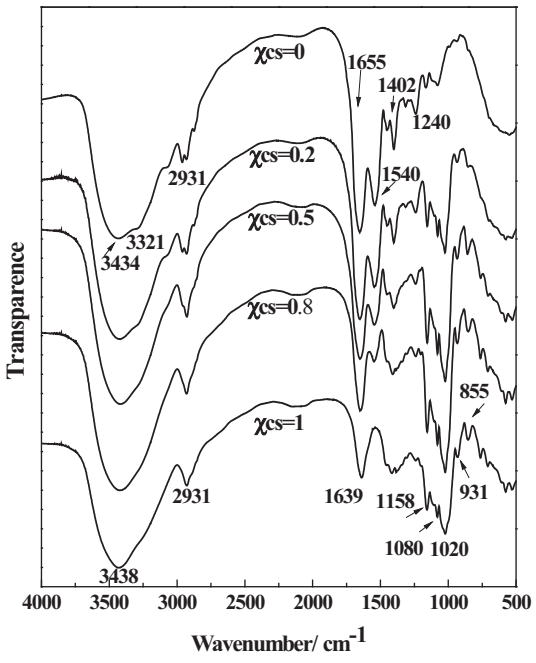

Fig. 4A. FTIR spectra of MP/CS composite gels with different χ_{cs}.

Amide bands I (1600–1700 cm^{-1}) and amide bands II (1500–1600 cm^{-1}) are generally employed to monitor the secondary structure conformation of a protein in various environments. In particular, amide I is considered to be the most reliable indicator of the secondary structure of proteins (Carbonaro & Nucara, 2010). In the CS spectrum, a peak (1639 cm^{-1}) was observed between 1600 and 1700 cm^{-1}, which could bring about a misestimation of the peak maximum and intensity in amide I of MP in the MP/CS composites, therefore the CS spectrum was subtracted from the MP spectrum in the presence of CS by the following equation:

$$\text{Spectrum MP} = \text{spectrum MP/CS} - (\gamma \times \text{spectrum CS}) \quad (6)$$

Given that the resulting MP spectrum was similar to that of pure MP, the value of γ was determined by the correlation coefficient R^2 between the two spectra. For the 1600–1750 cm^{-1} region, the highest R^2 of 0.9989 was obtained for MP/$CS_{\chi cs=0.8}$, MP/$CS_{\chi cs=0.5}$ and MP/$CS_{\chi cs=0.2}$ at γ = 0.8625, 0.3635 and 0.1067. Subsequently, Fourier self-deconvolution (FSD) and a multipeak fitting with Gaussian functions were applied to quantify the peak frequencies and the multicomponent peak areas in the 1600–1750 cm^{-1} region.

Fig. 4(B) shows the curve fitting of the Fourier deconvoluted amide bands I for MP/CS composites. Intense bands in the 1648–1660 cm^{-1} region are observed for α-helical conformation. A strong band between 1612 and 1641 cm^{-1} and a weaker band in the 1670–1694 cm^{-1} region are commonly ascribed to antiparallel β-sheets, whereas parallel β-sheet bands are reported between 1626 and 1640 cm^{-1}. β-turn and random coil structure are assigned to the bands within 1662–1684 cm^{-1} and 1640–1650 cm^{-1}, respectively (Carbonaro & Nucara, 2010). Table 2 summarizes the relative areas of the bands fit to the Fourier-deconvoluted spectra of the MP/CS composites (χ_{cs} 0–0.8), and each band was assigned to the component of the secondary structure according to previous data. Here, the two bands at approximately 1624 cm^{-1} and 1695 cm^{-1} can be ascribed to the stretching of the carbonyls of the β-sheet, and the relative area of the β-sheet decreased from 34.48 to 31.72% with increasing χ_{cs}, but without obvious differences ($P > 0.05$). The band at ~1650 cm^{-1} corresponding to the α-helix structure had a higher relative area in the MP/CS composites (χ_{cs} 0.8) than in other samples, verifying that the starch molecules can protect the protein against undesirable structure changes (Nawrocka et al., 2015). The band at approximately 1668 cm^{-1} is conventionally assigned to β-turns, which exhibited no significant change as χ_{cs} increased. The band at approximately 1642 cm^{-1} is typical of random coils, and the relative area of random coil significantly increased from 22.58 to 24.65% with increasing χ_{cs}. Overall, addition of CS and its fraction had no obvious influence on the secondary structure conformation of MP, which was in accord with previous results (Sun et al., 2014).

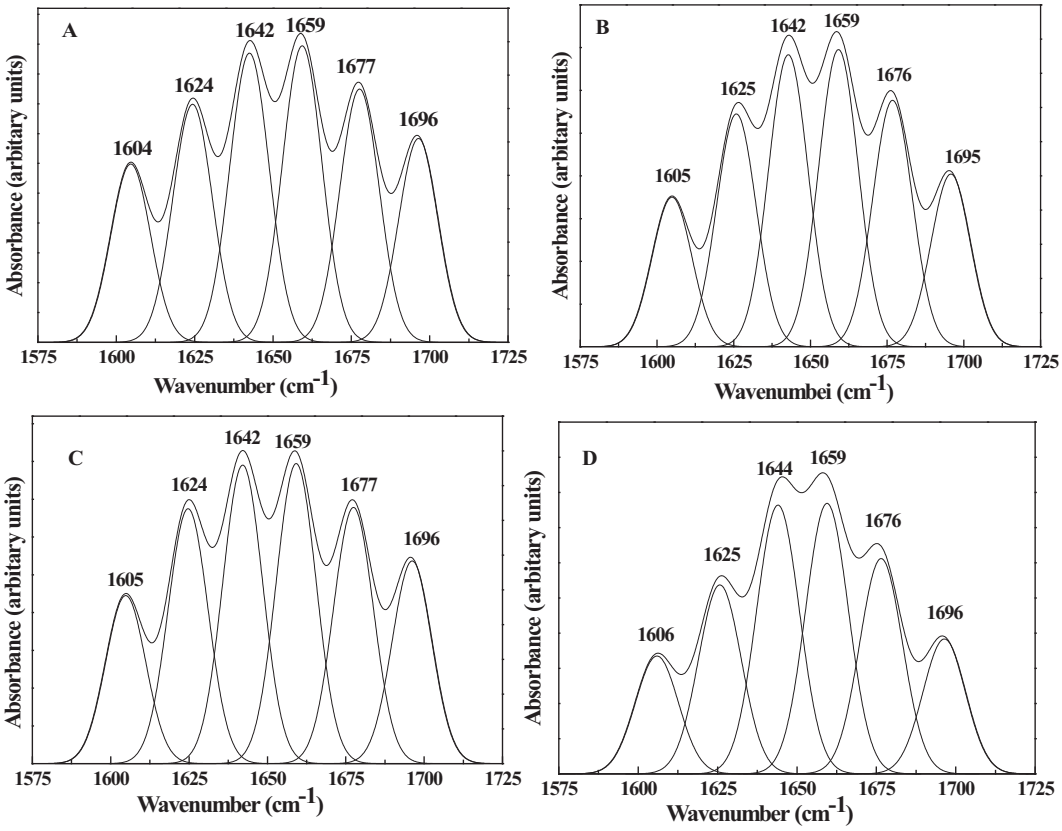

Fig. 4B. The curve fitting of Fourier deconvoluted amide bands I for MP/CS composites at different χ_{cs} (a–d). a–d: χ_{cs} = 0, 0.2, 0.5 and 0.8.

Table 2
The relative content of various MP secondary structure in MP/CS composites with different χ_{cs}.

Secondary structure	Range (cm^{-1})	CS fraction (χ_{cs})			
		0	0.2	0.5	0.8
α-helix	1648–1660	23.14 ± 0.01b	23.96 ± 0.02ab	22.79 ± 0.11b	24.47 ± 0.86a
β-sheet	1612–1641	18.60 ± 0.02ab	18.73 ± 0.04ab	19.39 ± 0.05a	18.02 ± 0.71b
	1626–1640	–	–	–	–
	1670–1694	15.88 ± 0.03a	13.86 ± 0.06a	15.44 ± 0.00a	13.70 ± 1.71a
Total		34.48 ± 0.05a	32.59 ± 0.11a	34.83 ± 0.05a	31.72 ± 2.42a
β-turn	1662–1684	19.80 ± 0.01a	19.95 ± 0.11a	19.65 ± 0.18a	19.16 ± 1.12a
Random coil	1640–1650	22.58 ± 0.04c	23.50 ± 0.00b	22.73 ± 0.04c	24.65 ± 0.44a

Mean values with different letters (a–c) of each row differ significantly ($P < 0.05$).

4. Conclusions

The CS fraction (χ_{cs}) was crucial for producing the heat-induced gelation characteristics and the microstructure of MP/CS composites. The morphology of the MP/CS composites underwent a transformation from MP gel → MP/CS elastic gel → MP/CS weak gel → CS viscous fluid as χ_{cs} increased from 0 to 1, and χ_{cs} 0.5 was a critical point for the transition of the gel from elastic to weak. The hardness, adhesiveness, gumminess and chewiness of the gel decreased significantly as χ_{cs} increased from 0 to 0.5. The rheological behaviour of the MP/CS composites was determined by the domination of either MP or CS. Moreover, MP and CS combined synergistically to affect G′ in all MP/CS composites, with the strongest effect at χ_{cs} 0.5 and 0.6. Such synergistic reinforcement could be interpreted by light microscopy with eosin/iodine double-staining: CS granules embedded in the MP gel could absorb water and swell during heating to compress the MP matrix and amylose released from the melted CS granules could interpenetrate with the MP molecules to form a semi-interpenetrating network. According to the creep-recovery data fit by Burger's model, a high recovery value of 76.5–82.3% was achieved for the composites, regardless of χ_{cs}, indicating their high elasticity and resistance to deformation. With increasing χ_{cs}, no chemical interaction between MP and CS was observed during heating, implying that CS addition and its fraction had no significant effect on the MP secondary structure.

Acknowledgements

This work was supported by the National Natural Science Foundation of China (31371796), Fundamental Research Funds for the Central Universities (2662015PY056), and the Application and Foundation Research Project of Wuhan Science and Technology Bureau of China (2014020101010068).

Appendix A. Supplementary data

Supplementary data associated with this article can be found, in the online version, at http://dx.doi.org/10.1016/j.foodchem.2016.09.068.

References

Alvarez, M. D., Fernández, C., Olivares, M. D., & Canet, W. (2012). A rheological characterisation of mashed potatoes enriched with soy protein isolate. *Food Chemistry, 133*(4), 1274–1282.

AOAC (1990). Official methods of analysis. 15th ed. Methods of 950.46, 984.13, 960.39 and 920.153. Association of Official Analytical Chemists, Washington, D.C.

Arfat, Y. A., & Benjakul, S. (2012). Gelling characteristics of surimi from yellow stripe trevally (*Selaroides leptolepis*). *International Aquatic Research, 4*(1), 1–13.

Ashwar, B. A., Gani, A., Shah, A., Wani, I. A., & Masoodi, F. A. (2015). Preparation, health benefits and applications of resistant starch– A review. *Starch/Starke, 67*, 1–15.

Carbonaro, M., & Nucara, A. (2010). Secondary structure of food proteins by Fourier transform spectroscopy in the mid-infrared region. *Amino Acids, 38*(3), 679–690.

Chanvrier, H., Colonna, P., Della Valle, G., & Lourdin, D. (2005). Structure and mechanical behaviour of corn flour and starch–zein based materials in the glassy state. *Carbohydrate Polymers, 59*(1), 109–119.

Chiang, P. Y., Li, J. Y., & Chen, M. L. (2009). Rheological characteristics and morphology of dialdehyde starch/meat composites during heating. *Journal of Food Science, 74*(2), E112–E119.

Di Monaco, R., Cavella, S., & Masi, P. (2008). Predicting sensory cohesiveness, hardness and springiness of solid foods from instrumental measurements. *Journal of Texture Studies, 39*(2), 129–149.

Ding, Y., Liu, R., Rong, J., Liu, Y., Zhao, S., & Xiong, S. (2012). Rheological behavior of heat-induced actomyosin gels from yellowcheek carp and grass carp. *European Food Research and Technology, 235*(2), 245–251.

Foegeding, E. A., Allen, C. E., & Dayton, W. R. (1986). Effect of heating rate on thermally formed myosin, fibrinogen and albumin gels. *Journal of Food Science, 51*, 104–108.

Friedman, H. H., Whitney, J. E., & Szczesniak, A. S. (1963). The texturometer-a new instrument for objective texture measurement. *Journal of Food Science, 28*(4), 390–396.

Hunt, A., Getty, K. J. K., & Park, J. W. (2009). Roles of starch in surimi seafood: A review. *Food Reviews International, 25*(4), 299–312.

Jekle, M., Mühlberger, K., & Becker, T. (2016). Starch–gluten interactions during gelatinization and its functionality in dough like model systems. *Food Hydrocolloids, 54*, 196–201.

Jia, D., Huang, Q., & Xiong, S. (2016). Chemical interactions and gel properties of black carp actomyosin affected by MTGase and their relationships. *Food Chemistry, 196*, 1180–1187.

Jiang, S. T., Lee, B. L., Tsao, C. Y., & Li, J. J. (1997). Mackerel cathepsins B and L effects on thermal degradation of surimi. *Journal of Food Science, 62*(2), 310–315.

Joshi, M., Aldred, P., Panozzo, J. F., Kasapis, S., & Adhikari, B. (2014). Rheological and microstructural characteristics of lentil starch–lentil protein composite pastes and gels. *Food Hydrocolloids, 35*, 226–237.

Juszczak, L., Witczak, T., Ziobro, R., Korusc, J., Cieślikd, E., & Witczakb, M. (2012). Effect of inulin on rheological and thermal properties of gluten-free dough. *Carbohydrate Polymers, 90*(1), 353–360.

Kacurakova, M., Capek, P., Sasinkova, V., Wellnerb, N., & Ebringerová, A. (2000). FT-IR study of plant cell wall model compounds: Pectic polysaccharides and hemicelluloses. *Carbohydrate Polymers, 43*(2), 195–203.

Kaddour, A. A., Mondet, M., & Cuq, B. (2008). Description of chemical changes implied during bread dough mixing by FT-ATR mid-infrared spectroscopy. *Cereal Chemistry, 85*(5), 673–678.

Kim, J. M., & Lee, C. M. (1987). Effect of starch of textural properties of surimi gel. *Journal of Food Science, 52*(3), 722–725.

Li, J. Y., & Yeh, A. I. (2002). Functions of starch in formation of starch/meat composite during heating. *Journal of Texture Studies, 33*(4), 341–366.

Li, J. Y., & Yeh, A. I. (2003). Gelation properties and morphology of heat-induced starch/salt-soluble protein composites. *Journal of Food Science, 68*(2), 571–579.

Li, J. Y., Yeh, A. I., & Fan, K. L. (2007). Gelation characteristics and morphology of corn starch/soy protein concentrate composites during heating. *Journal of Food Engineering, 78*(4), 1240–1247.

Mejia, C. D., Mauer, L. J., & Hamaker, B. R. (2007). Similarities and differences in secondary structure of viscoelastic polymers of maize α-zein and wheat gluten proteins. *Journal of Cereal Science, 45*(3), 353–359.

Muriel-Galet, V., López-Carballo, G., Gavara, R., & Hernández-Muño, P. (2015). Antimicrobial effectiveness of lauroyl arginate incorporated into ethylene vinyl alcohol copolymers to extend the shelf-life of chicken stock and surimi sticks. *Food and Bioprocess Technology, 8*(1), 208–217.

Nawrocka, A., Szymańska-Chargot, M., Miś, A., Ptaszyńska, A. A., Kowalski, R., Waśko, P., & Gruszecki, W. I. (2015). Influence of dietary fibre on gluten proteins structure-a study on model flour with application of FT-Raman spectroscopy. *Journal of Raman Spectroscopy, 46*(3), 309–316.

Nuanmano, S., Prodpran, T., & Benjakul, S. (2015). Potential use of gelatin hydrolysate as plasticizer in fish myofibrillar protein film. *Food Hydrocolloids, 47*, 61–68.

Onyango, C., Mutungi, C., Unbehend, G., & Lindhauerc, M. G. (2010). Rheological and baking characteristics of batter and bread prepared from pregelatinised cassava starch and sorghum and modified using microbial transglutaminase. *Journal of Food Engineering, 97*(4), 465–470.

Park, J. W. (2005). *Surimi and surimi seafood* (2nd ed.). USA: CRC Press (Chapter 13).

Rao, M. A., Kash, S. F., Cooley, H. J., & Barnard, J. (1987). Desktop computer based collection and analysis of creep-compliance data on fluid foods. *Journal of Texture Studies, 18*(4), 405–413.

Rashid, I., Al Omari, M. H., Leharne, S. A., Chowdhry, B. Z., & Badwan, A. (2012). Starch gelatinization using sodium silicate: FTIR, DSC, XRPD, and NMR studies. *Starch-Stärke, 64*(9), 713–728.

Ronda, F., Pérez-Quirce, S., Angioloni, A., & Collar, C. (2013). Impact of viscous dietary fibres on the viscoelastic behaviour of gluten-free formulated rice doughs: a fundamental and empirical rheological approach. *Food Hydrocolloids, 32*(2), 252–262.

Sun, F., Huang, Q., Hu, T., Xiong, S., & Zhao, S. (2014). Effects and mechanism of modified starches on the gel properties of myofibrillar protein from grass carp. *International Journal of Biological Macromolecules, 64*, 17–24.

Van Ness, H. C., & Abbott, M. M. (1982). *Classical thermodynamics of nonelectrolyte solutions with applications to phase equilibria* (pp. 184–261). New York: McGraw-Hill.

Wu, C., Yuan, C., Chen, S., Liu, D., Ye, X., & Hu, Y. (2015). The effect of curdlan on the rheological properties of restructured ribbonfish (*Trichiurus* spp.) meat gel. *Food Chemistry, 179*, 222–231.

Yang, H., & Park, J. W. (1998). Effects of starch properties and thermal-processing conditions on surimi–starch gels. *LWT-Food Science and Technology, 31*(4), 344–353.

Yang, Z., Wang, W., Wang, H., & Ye, Q. (2014). Effects of a highly resistant rice starch and pre-incubation temperatures on the physicochemical properties of surimi gel from grass carp (*Ctenopharyn Odon Idellus*). *Food Chemistry, 145*, 212–219.

Yongsawatdigul, J., Worratao, A., & Park, J. W. (2002). Effect of endogenous transglutaminase on threadfin bream surimi gelation. *Journal of Food Science, 67*(9), 3258–3263.

Ziegler, G. R., & Foegeding, E. A. (1990). The gelation of proteins. *Advances in Food and Nutrition Research, 34*, 203–298.